

Predictability of the thermally-driven laboratory rotating annulus

R. M. B. Young and P. L. Read

Supporting Information

Contents

1	Datafile expf1	1
2	Climate distributions	1
3	Testing the breeding parameters for the main FANFARE ensemble	1
4	Choosing Ω and ΔT to use in the model	5
5	Imperial College Ocean Model (ICOM) simulations	5
6	Flow diagrams for the various stages in FANFARE	6
7	Additional results figures	6

1 Datafile expf1

Datafile expf1 (climate distributions only) contained 1,389,584 raw and 1,387,295 processed observations, in 2,150 processed datasets (430 at each of five vertical levels). The data processing is described in [Young and Read \[2013\]](#). Subset 1 had missing data at 9900 s and subset 2 at 4405 s and 9900 s. Figure [S1](#) shows the rotation rate and temperature difference between the cylinders in this datafile.

2 Climate distributions

The four datafiles expf1, expf2, expf5, and expf6 were used to produce climatological distributions of horizontal velocity at each rotation rate available in the data (used to measure forecast skill). The climate data consists of radial velocity, azimuthal velocity, and velocity magnitude distributions at each vertical level as a function of radius. Because of the rotational symmetry of the experiment the climatological distribution has azimuthal symmetry, so the values are a function of (R, z) only. At each level at 72 regularly-spaced radial points the distribution of u and v velocities was calculated, along with the climate mean and variance. Table [S1](#) lists the regimes for which climate distributions were produced, and Fig. [S2](#) shows an example. At vertical positions where no observations are available and climate values are required, the climate values were interpolated using a cubic spline (IDL routine *interpol*), fixing zero at the upper and lower boundaries.

3 Testing the breeding parameters for the main FANFARE ensemble

Before forecasts were run, the parameters were optimised like they were in our perfect model scenario (PMS) and assimilation experiments [[Young and Read, 2008a, 2013](#)]. Unlike the PMS these parameters were the same for both the breeding and forecast stages. The following parameters were tested:

The **size of the initial perturbation as a fraction of the RMS climate variance**, F , should be optimised for the best RMS improvement in the ensemble mean over the control in subsequent forecasts. This is tested by varying F with constant Δt_B and N_B , and measuring the ratio of RMS errors in the forecasts; the smaller the ratio the better.

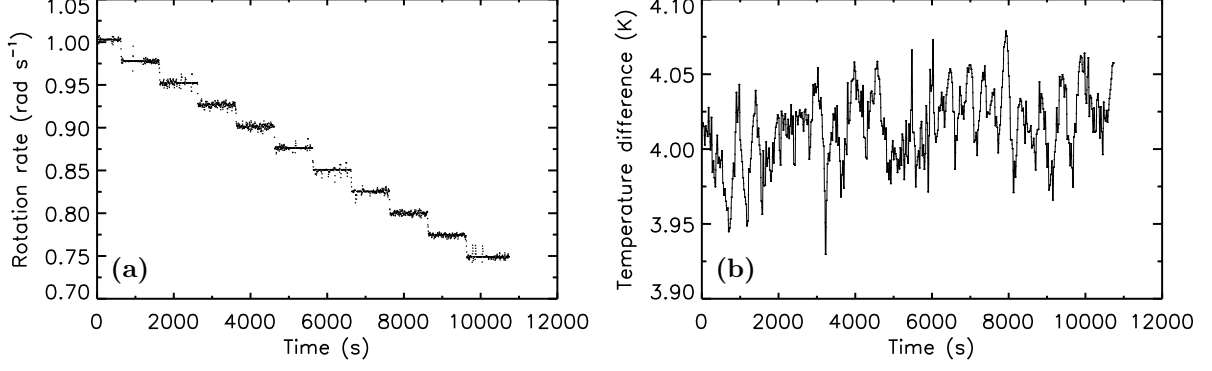


Figure S1: (a) Rotation rate Ω and (b) temperature difference $\Delta T = T_b - T_a$ between the cylinders as a function of time for datafile expf1. Note that the scatter probably represents measurement error and not real scatter in the forcing.

Regular Ω (rad s ⁻¹)	Datafiles (ΔT (K))	Chaotic Ω (rad s ⁻¹)	Datafiles (ΔT (K))
1.000	expf1 (4.00)	2.2	expf5 (4.02)
0.975	expf1 (4.00)	2.3	expf5 (4.02)
0.950	expf1 (4.01)	2.4	expf5 (4.02)
0.925	expf1 (4.01)	2.5	expf5 (4.02)
0.900	expf1 (4.02)	2.6	expf5 (4.02) / expf6 (4.02)
0.875	expf1 (4.00) / expf2 (4.07)	2.7	expf6 (4.02)
0.850	expf1 (4.02) / expf2 (4.04)	2.8	expf6 (4.02)
0.825	expf1 (4.03) / expf2 (4.03)	2.9	expf6 (4.02)
0.800	expf1 (4.03) / expf2 (4.04)	3.0	expf6 (4.02)
0.775	expf1 (4.02) / expf2 (4.05)	3.1	expf6 (4.02)
0.750	expf1 (4.03) / expf2 (4.05)		

Table S1: List of annulus climate distributions. The distributions are split into two parts: regular regime distributions using expf1 and expf2, and chaotic regime distributions using expf5 and expf6. Climate distributions are available at each rotation rate used in the four datafiles. The experimental datafiles which contribute to each distribution are indicated with an approximate value for ΔT in each case; if two are used then both are listed.

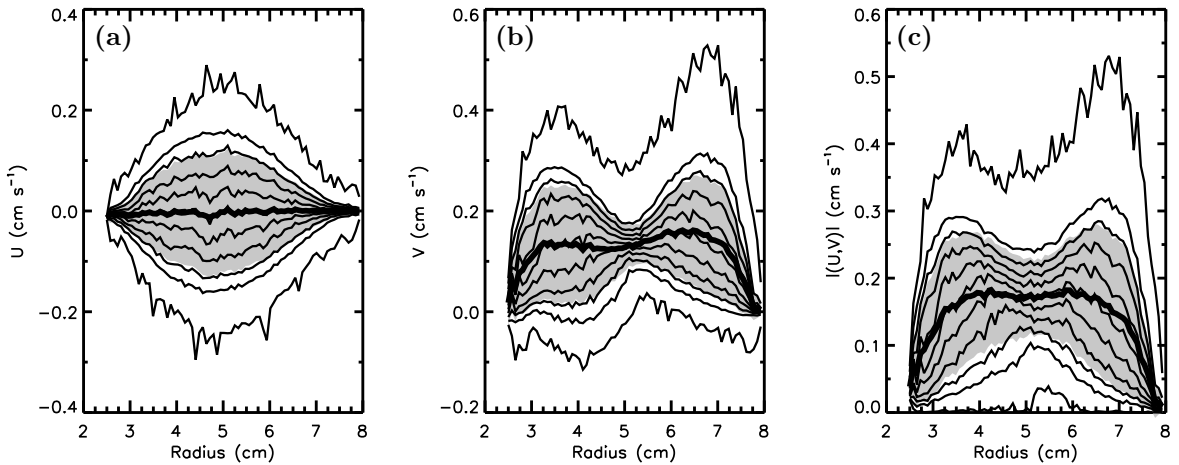


Figure S2: Example (a) u , (b) v , and (c) $\sqrt{u^2 + v^2}$ climate distributions at $\Omega = 2.4 \text{ rad s}^{-1}$ / $z = 9.7 \text{ cm}$ in the 3SV data. The thin lines represent percentiles 0%, 10%, 20%, ..., 100% of the climate distribution. The thick line is the climate mean and the shaded area represents the mean \pm standard deviation.

Regime	Datafile	Ω (rad s ⁻¹)	bg (s)	t_0 (s)	t_1 (s)	t_2 (s)	t_3 (s)	Δt_{short} (s)	N_{short}
3SV	expf5	2.5	1500	6390	6400	7000	7400	1.0	5
2S	expf2	0.775	1500	7975	8000	8600	8900	2.5	2

(a) Parameters kept constant in each regime. $\Delta t_{\text{long}} = 5.0$ s and $N_{\text{before}} = 10$ in both cases. bg is the length of the MORALS initialisation run.

Regime	Varying F :			Varying Δt_B and N_B :	
	Δt_B	N_B	F	F	$[\Delta t_B, N_B]$
3SV	60	10	0.368, 0.223, 0.135 0.0498, 0.0183, 0.00674	0.135	[10, 60], [30, 20], [60, 10], [100, 6]
2S	30	20	0.368, 0.135, 0.0498	0.135	[10, 60], [30, 20], [60, 10]

(b) Parameters that were varied.

Table S2: Parameters used to test the breeding parameters for FANFARE. The F values correspond to e^{-1} , $e^{-3/2}$, e^{-2} , e^{-3} , e^{-4} , and e^{-5} .

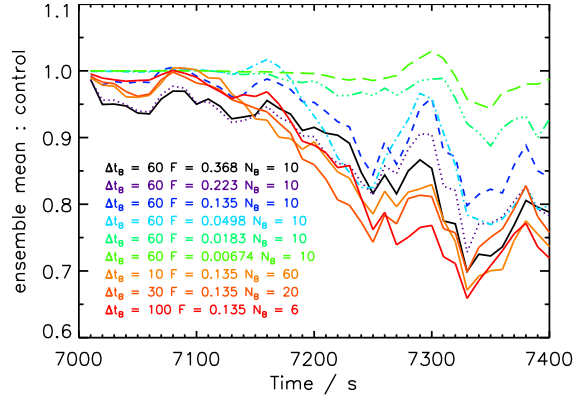
The **time between rescaling of the BVs**, Δt_B , should be shorter than the time the perturbation takes to saturate, and it should be large enough for the perturbations to become nonlinear. The first condition is tested by varying Δt_B with constant F and N_B and measuring the cycle growth g_c (main text, Eq. 5); Δt_B should be short enough so that g_c does not exceed $1/F$ during a single cycle. The second condition is tested by varying Δt_B at constant F and N_B and measuring the relative nonlinearity R_{NL} (main text, Eq. 11) and the anticorrelation l [Gilmour et al., 2001, not shown]; Δt_B should be long enough such that $R_{\text{NL}} > 0.2$ or $l < 0.7$.

The breeding stage builds up a coherent set of BVs over a **number of cycles in the breeding stage**, N_B . For the BVs to be coherent they should cover the range of analysis error and be independent of the initial Gaussian perturbations. The time this takes is estimated by measuring g_c as a function of time: once this equilibrates at a constant value the shape of the BV has settled down to a steady pattern, independent of the initial perturbation. Ideally N_B should be as small as possible because it determines the amount of data available for the subsequent forecasts.

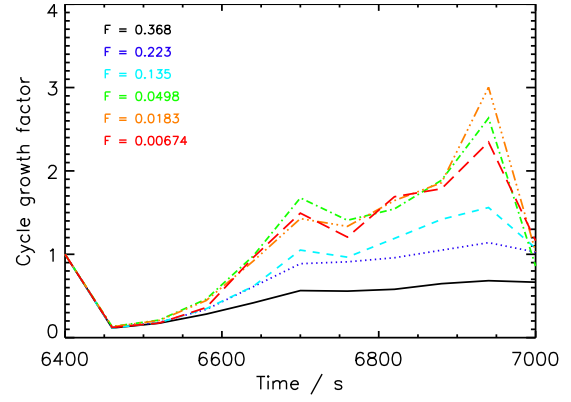
A series of FANFARE forecasts were made to test these parameters in both the chaotic (3SV) and regular (2S) regimes. The parameters kept constant in each of these runs are listed in Table S2a (the positions of these runs in the observational datafiles are shown in Fig. 5 in the main text. Two sets of runs were run in each regime; one varying F with Δt_B and N_B fixed, and one varying Δt_B and N_B with F fixed (keeping $\Delta t_B \times N_B$ constant). The parameters varied in each test are listed in Table S2b.

Tests with 3SV data The ratio of RMS errors are shown in Fig. S3a. Varying F found that higher F leads to a better ensemble mean. Varying Δt_B did not show any general trend. To test saturation of the BVs, cycle growth factor is plotted in Figs S3b and S3c for varying F and Δt_B respectively. For saturation, the cycle growth factor must exceed $1/F$ during one cycle, and this condition is not met in any cases. To test nonlinearity, the R_{NL} plots are shown in Figs S3d and S3e. Varying Δt_B exceeded $R_{\text{NL}} = 0.2$ in all cases, and also for almost all values of F ; in general a higher Δt_B or higher F means higher R_{NL} . The anticorrelation plots are not shown, but they give the same result. Hence all the Δt_B values passed the tests for nonlinearity and non-saturation. To choose between them, Fig. S3c shows how long g_c takes to equilibrate with varying Δt_B and N_B . Of the values shown, only $\Delta t_B = 10$ s and 30 s equilibrate during the breeding stage, so values above this are rejected. The time taken to equilibrate is shorter for lower Δt_B but the computational expense increases, so to compromise $\Delta t_B = 20$ s is used. The BV generation stage is 500 s long ($N_B = 25$) to allow ample time for equilibration. To choose a suitable value for F , the RMS errors for each test over the forecast stage are shown in Fig. S3f. In general, higher F means lower RMS error. Both $F = 0.368$ and 0.223 perform similarly in the forecast stage and have similar R_{NL} and l . $F = 0.223$ exceeds $g_c = 1$ (just) but $F = 0.368$ does not, and ideally BVs should grow on average over the course of a cycle, so $F = 0.2$ was chosen for use in the forecasts.

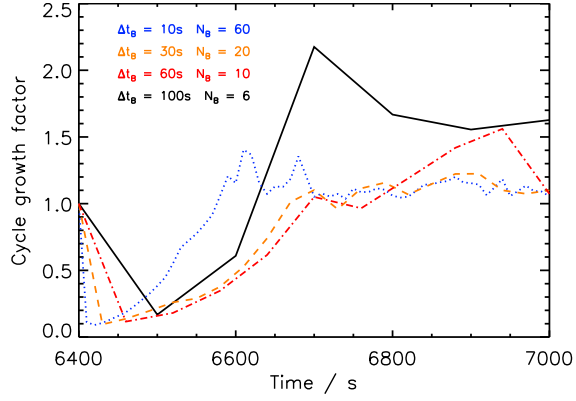
Tests with 2S data The tests in the 2S dataset all had very similar results. In general, higher F lead to higher R_{NL} and marginally lower l , but the conditions for nonlinearity are not fulfilled in any case. The growth was less than 0.04 in all cases after the first cycle, and this value does not vary much at all



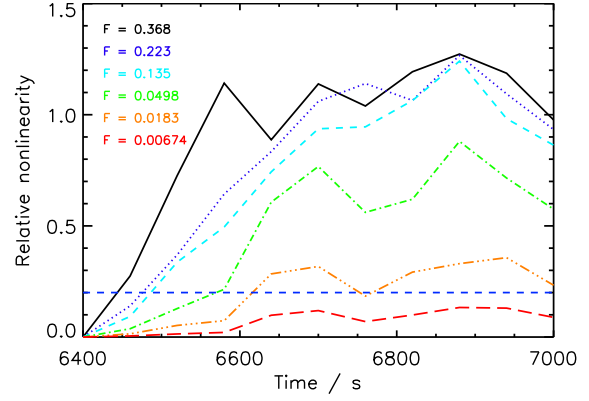
(a) Ratio of RMS errors



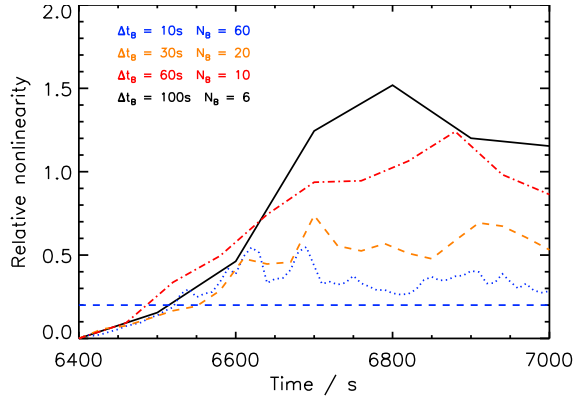
(b) Growth rate, varying F



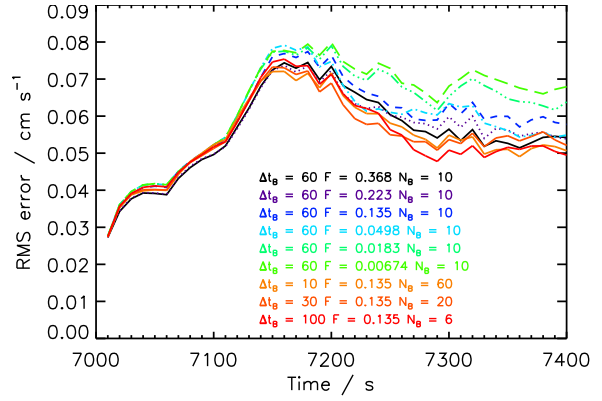
(c) Growth rate, varying Δt_B



(d) R_{NL} , varying F



(e) R_{NL} , varying Δt_B



(f) RMS error

Figure S3: FANFARE parameter test results for the 3SV regime. Only u data at $z = 9.7$ cm is shown, for brevity.

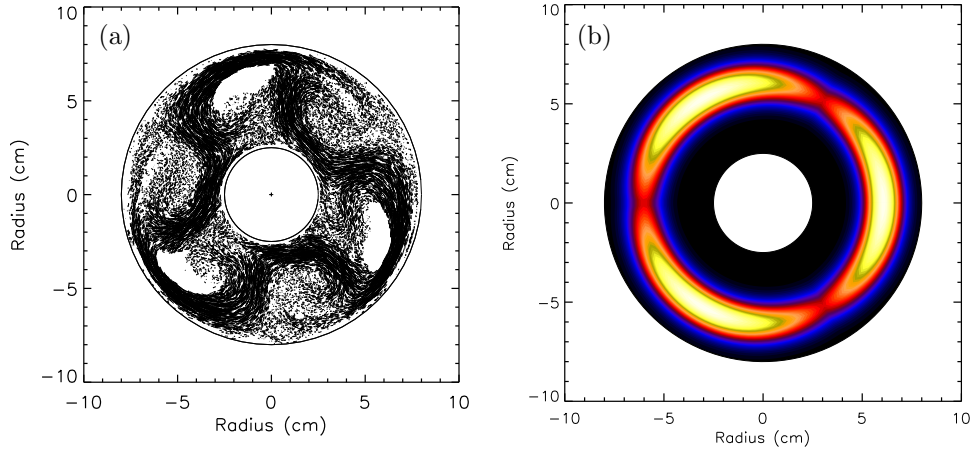


Figure S4: (a) Streaklines showing observations at datafile expf6 at $z = 9.7$ cm between 10 500–10 700 s, and (b) bottom topography used in the ICOM with topography simulation to represent the effect of the data holes. The lightest colour corresponds to 3 mm.

with F or Δt_B . The growth factor equilibrates after about 300 s. So, to keep things simple, the same parameters as 3SV were used, but the breeding stage was slightly shorter.

4 Choosing Ω and ΔT to use in the model

At first glance the most obvious values of Ω and ΔT to use in MORALS when forecasting experimental data are the values measured with the observations at the start of the forecast (Fig. 5 in main text), combined with Ω and ΔT shifts from observation to simulation, estimated to be $\Omega_{\text{shift}} = -0.11 \text{ rad s}^{-1}$ and $\Delta T_{\text{shift}} = 0.0 \text{ degC}$ for this annulus geometry and fluid [Young and Read, 2008b].

But because Ω and ΔT change over time (as can be seen in Fig. S1, and Fig. 5 in the main text) they should reflect the *expected* values of Ω and ΔT over the course of the subsequent observations. Although the values do not change significantly between two assimilations, over a breeding cycle or forecast they can change considerably, and the values of Ω and ΔT at the start may bias the forecast later on if they are at the edge of the range of Ω and ΔT over the subsequent observations. As there are no prognostic equations for Ω and ΔT , and to avoid using information from the future, the best estimates of future Ω and ΔT are their mean values from observations prior to the start of the forecasts. On this basis the following Ω and ΔT were used in each situation, before Ω_{shift} and ΔT_{shift} were applied:

MORALS initialization: Either user-specified Ω and ΔT , or the measured values at $t = t_0$. Operationally there would be no knowledge of future Ω and ΔT so it is acceptable to use pre-specified values based on what it is thought the system will do.

Assimilation: The time between assimilations is short enough for Ω and ΔT to remain approximately constant, so measurements at the analysis time ($t = t_a$) are used.

BV generation: Because Ω and ΔT could change significantly over the course of one cycle, the mean values over the observations up to the start of that cycle are used ($t_0 \rightarrow t_a$).

Main forecasts: The mean of the measured Ω and ΔT values over the assimilation stage $t_0 \rightarrow t_2$ was used, as the best *a priori* estimate of what the values will do in the future.

5 Imperial College Ocean Model (ICOM) simulations

ICOM was run in ocean mode, with no mesh adaptivity, using the same grid as MORALS. Two-dimensional Gaussian topography with three ‘hills’ was added to one simulation (Fig. S4):

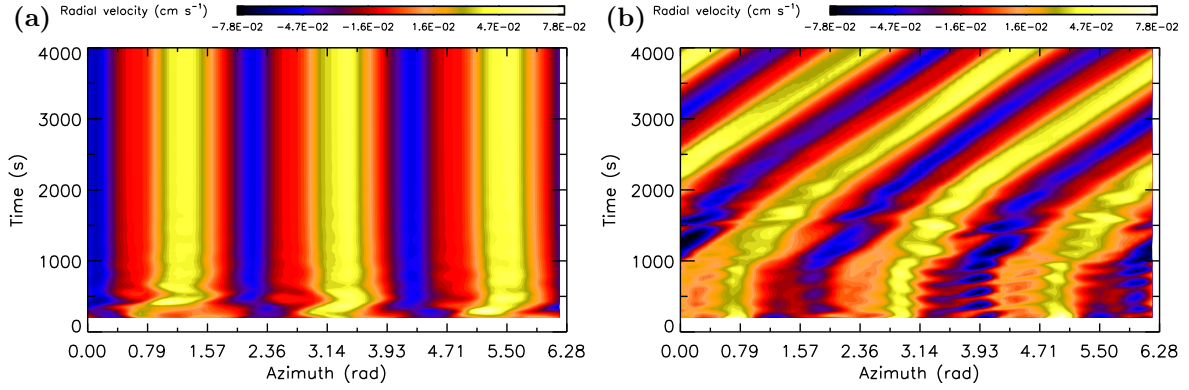


Figure S5: Hovmöller plots of radial velocity at mid-height / mid-radius from ICOM simulations with (a) and without (b) bottom topography. The first 200 s are omitted to enhance colour contrast. Topography peaks are at azimuth 0.00, 2.09, and 4.19 rad. A $m = 3$ bias was applied up to $t = 1000$ s in the plot on the right. Data produced by James Maddison.

$$h(R, R\phi) = H \exp \left[-\frac{(R - R_\mu)^2}{2\sigma_R^2} - \frac{R(\phi - \phi_\mu)^2}{2\sigma_{R\phi}^2} \right] \quad (1)$$

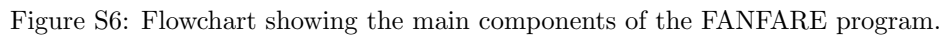
where $H = 0.3$ cm is the estimated height of the topography, $\sigma_R = 0.67$ cm and $\sigma_{R\phi} = 1.95$ cm are the standard deviations in the radial and azimuthal directions, $R_\mu = 6.07$ cm is the radius at the topography peak, and $\phi_\mu = 0$ rad, $2\pi/3$ rad, $4\pi/3$ rad. The two runs used $\Omega = 3.0$ rad s $^{-1}$ and $\Delta T = 4.02$ K. Both started from an initial condition produced by a MORALS 2D simulation. In the run without topography, an artificial bias was required at the start to stimulate wavenumber-3 behaviour, taking the form of an extra term $-\lambda_0 |\sin 3\phi| t$ in the heat transport equation, with $\lambda_0 = 0.05$ for $t < 500$ s, $\lambda_0 = 0.1(1 - 0.001t)$ for $500 \text{ s} \leq t \leq 1000$ s, and $\lambda_0 = 0$ thereafter. Results are shown in Fig. S5. Topography causes the wave to become locked to the tank after about 500 s.

6 Flow diagrams for the various stages in FANFARE

Figures S6–S8 show flow diagrams for the various parts of the forecasting framework. Figure S6 shows the main components, Fig. S7 shows the breeding vector generation stage, and Fig. S8 shows the forecast stage. The symbols are from IBM Corp. [1969] — rectangle: processing step, parallelogram: I/O, diamond: decision, cylinder: data file, oval: start/end, arrow: flow of program control / information, circle/cross: addition operator.

7 Additional results figures

We include here complete sets of figures from each of the forecasts, of which only a few are shown in the main text. Figure S9 shows spaghetti plots, Fig. S10 shows ensemble forecasts, Fig. S11 shows Hovmöller plots, and Fig. S12 shows azimuthal velocity breeding vectors.



R. M. B. Young and P. L. Read. Data assimilation in the laboratory using a rotating annulus experiment. *Q. J. R. Meteorol. Soc.*, 139:1488–1504, 2013. doi: 10.1002/qj.2061.

R M B Young and P L Read. Breeding and predictability in the baroclinic rotating annulus using a perfect model. *Nonlinear Process. Geophys.*, 15:469–487, 2008a. doi: 10.5194/npg-15-469-2008.

Isla Gilmour, Leonard A Smith, and Roberto Buizza. Linear Regime Duration: Is 24 Hours a Long Time in Synoptic Weather Forecasting? *J. Atmos. Sci.*, 58:3525–3539, 2001. doi: 10.1175/1520-0469(2001)058\$(\$3525:LRDIHA\$)\$2.0.CO;2.

R M B Young and P L Read. Flow transitions resembling bifurcations of the logistic map in simulations of the baroclinic rotating annulus. *Phys. D*, 237:2251–2262, 2008b. doi: 10.1016/j.physd.2008.02.014.

IBM Corp. *IBM Data Processing Techniques: Flowcharting Techniques*, 1969. Internal ref. C20-8152-1. 40 pages.

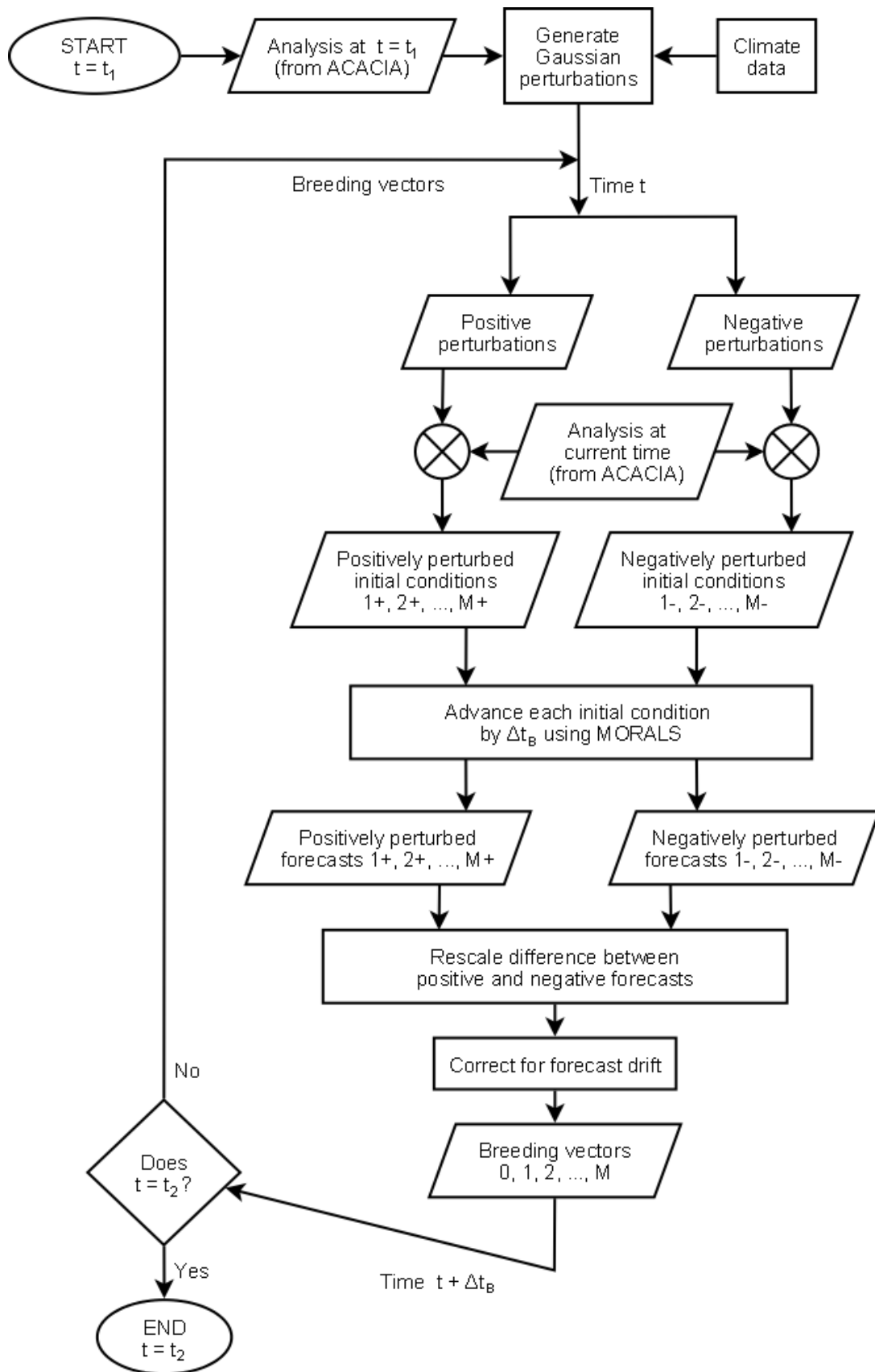


Figure S7: Flowchart of the FANFARE breeding vector generation stage.

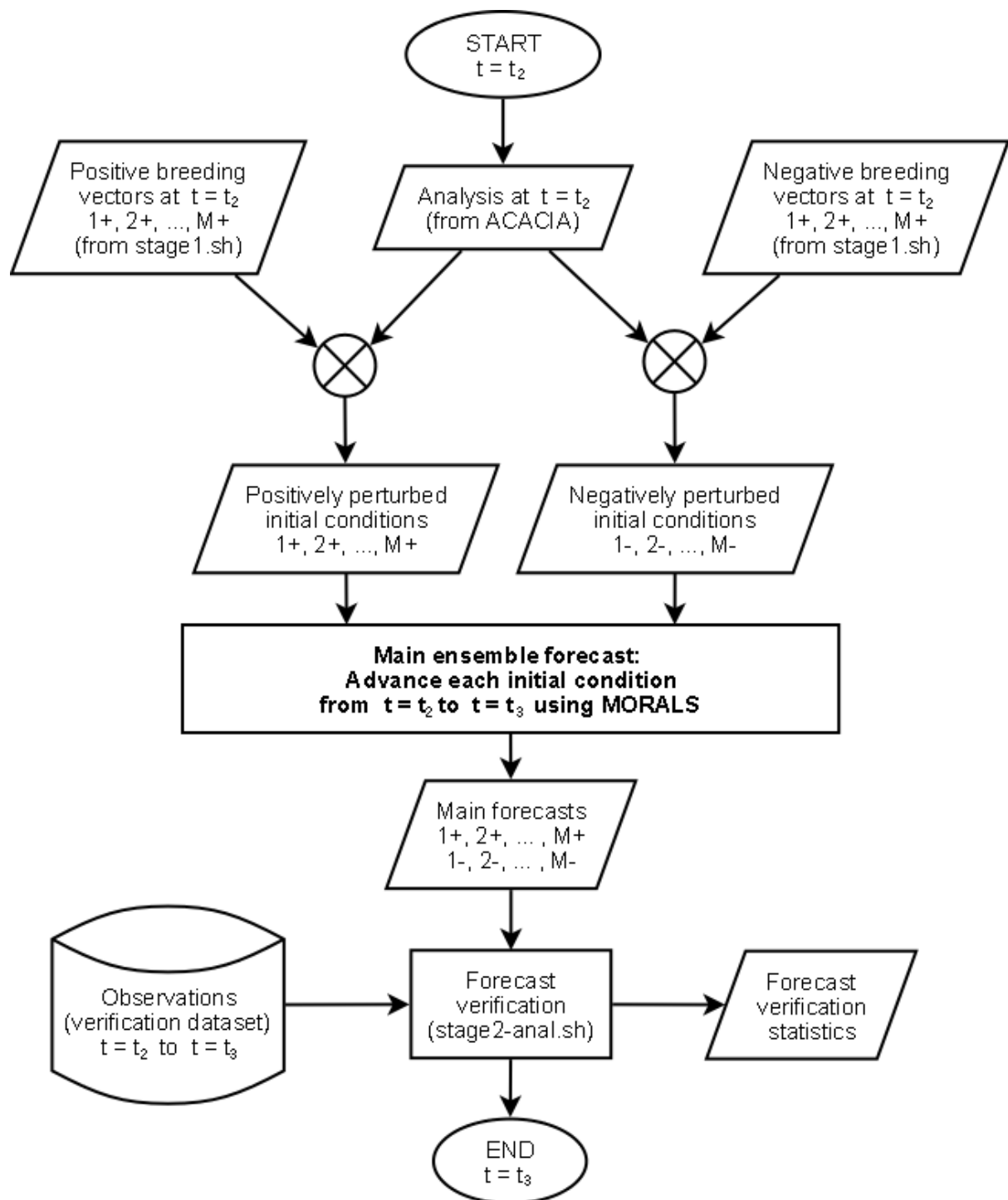


Figure S8: Flowchart of the forecast stage.

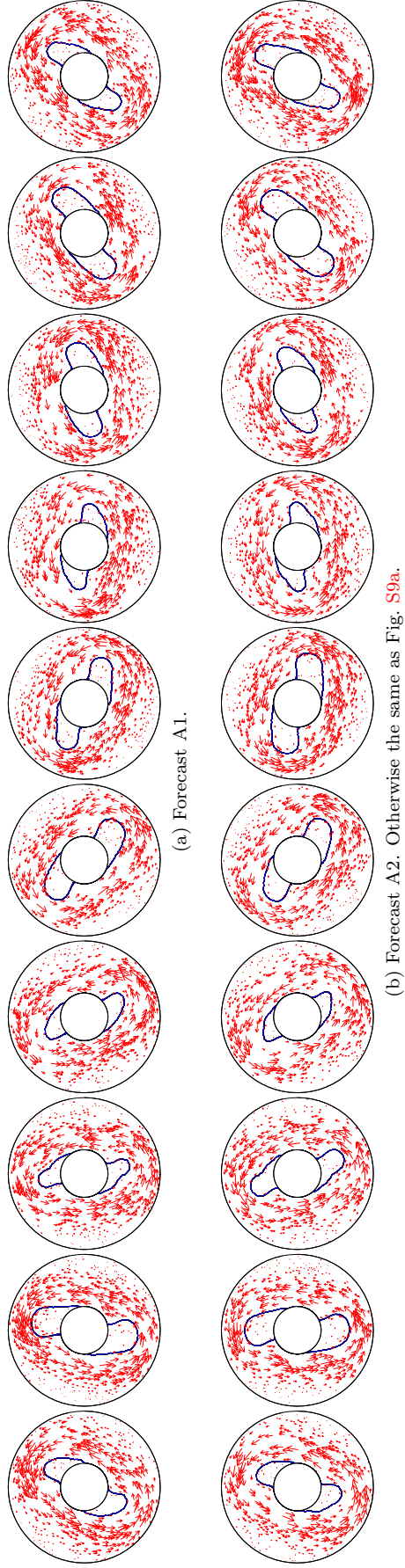
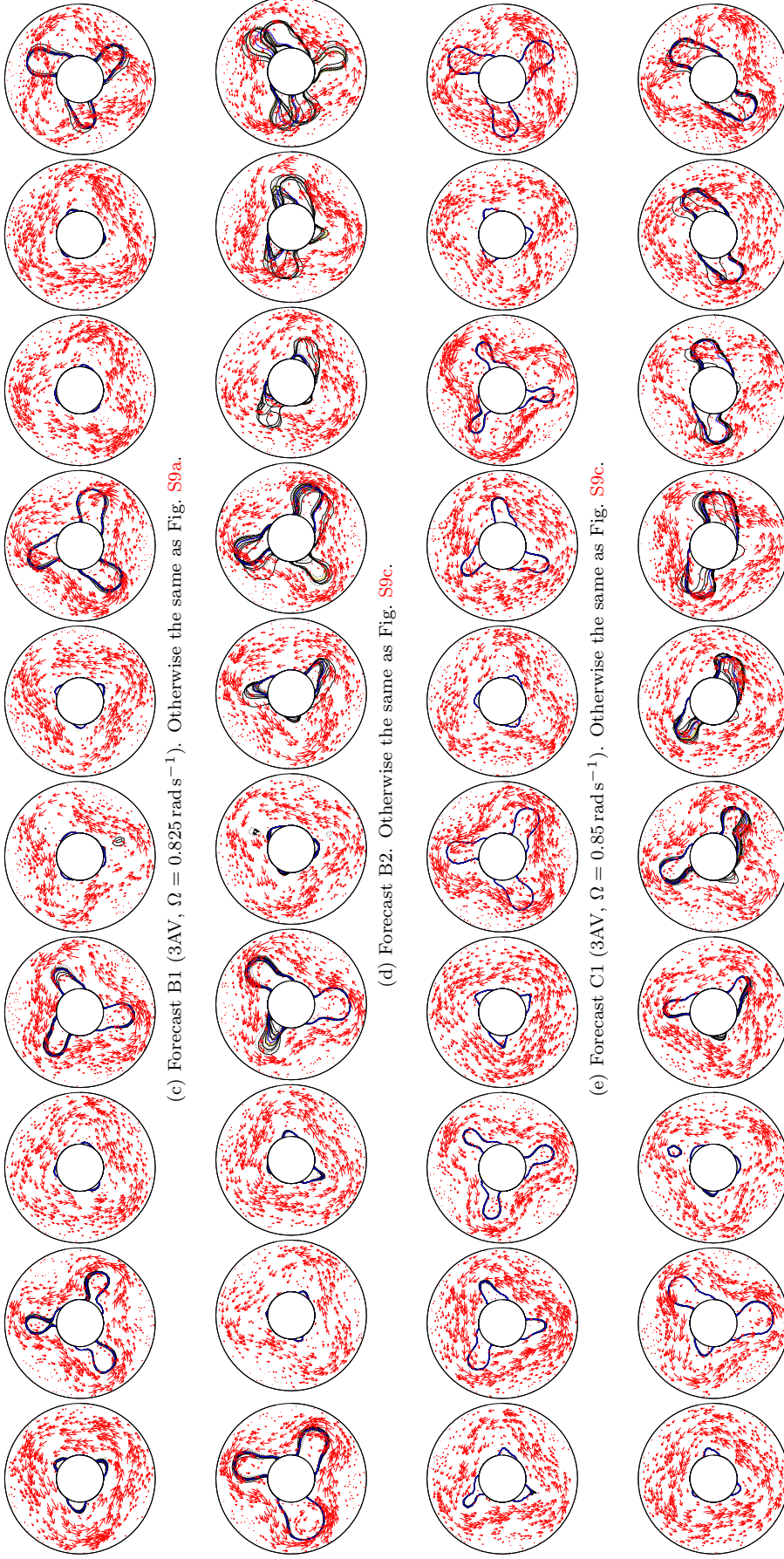


Figure S9: Sequence of spaghetti plots showing forecast A (2S, $\Omega = 0.775 \text{ rad s}^{-1}$) at $z = 9.7 \text{ cm}$. Frames are separated by 100 s, and the final frame is at $t_2 + 970 \text{ s}$. Each frame shows the $\Psi = 0$ streamfunction contour for each of the positive ensemble members (black solid), negative ensemble members (black dotted), control forecast (brown solid), ensemble mean (blue solid), and observed vector velocity field (red arrows).



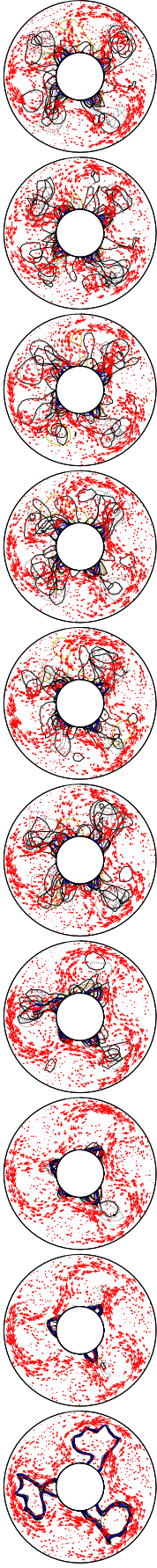
(c) Forecast B1 (3AV, $\Omega = 0.825 \text{ rad s}^{-1}$). Otherwise the same as Fig. S9a.

(d) Forecast B2. Otherwise the same as Fig. S9c.

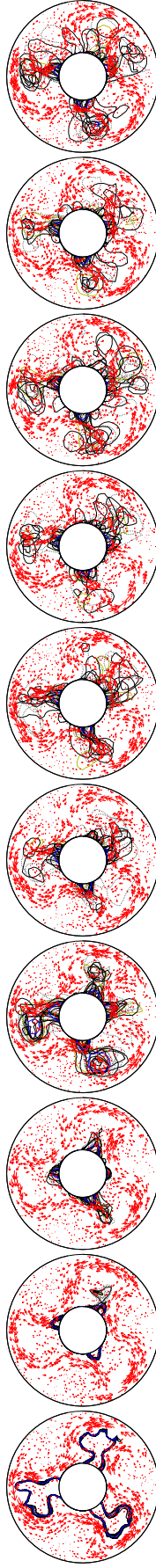
(e) Forecast C1 (3AV, $\Omega = 0.85 \text{ rad s}^{-1}$). Otherwise the same as Fig. S9c.

(f) Forecast C2. Otherwise the same as Fig. S9e.

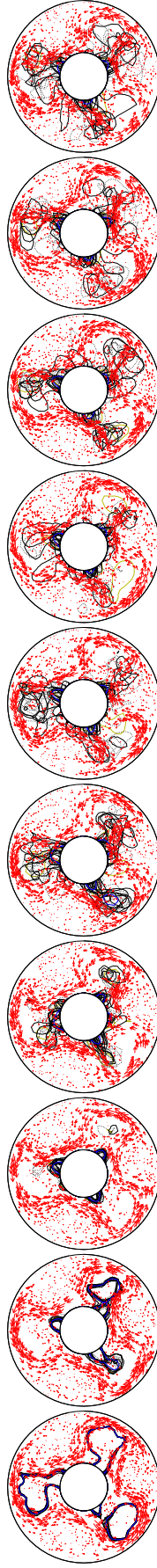
Figure S9: Spaghetti plots for forecasts B and C (3AV).



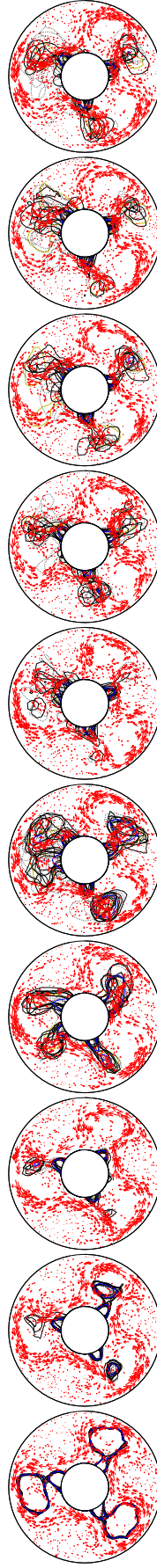
(g) Forecast D1 (3SV, $\Omega = 2.4 \text{ rad s}^{-1}$). Frames are separated by 60 s, and the final frame is at $t_2 + 550 \text{ s}$. Otherwise the same as Fig. S9a.



(h) Forecast D2. Otherwise the same as Fig. S9g.

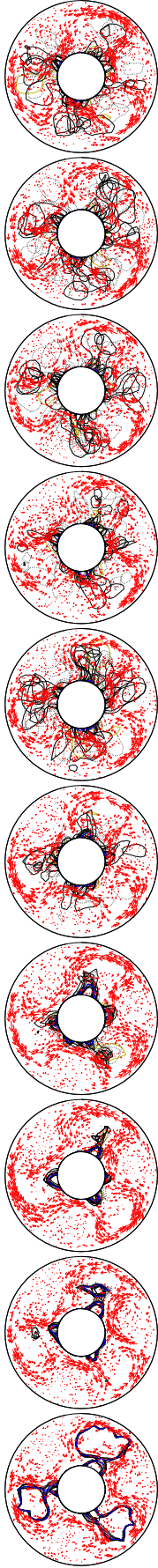


(i) Forecast E1 (3SV, $\Omega = 2.6 \text{ rad s}^{-1}$). Otherwise the same as Fig. S9g.

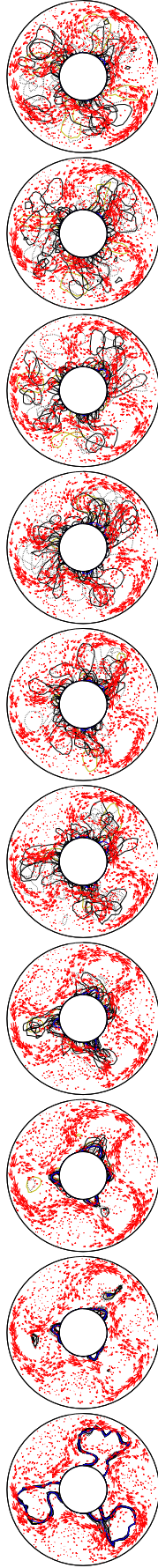


(j) Forecast E2. Otherwise the same as Fig. S9i.

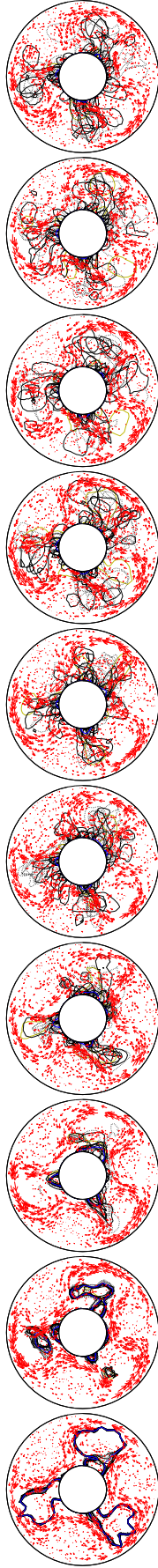
Figure S9: Spaghetti plots for forecasts D and E (3SV).



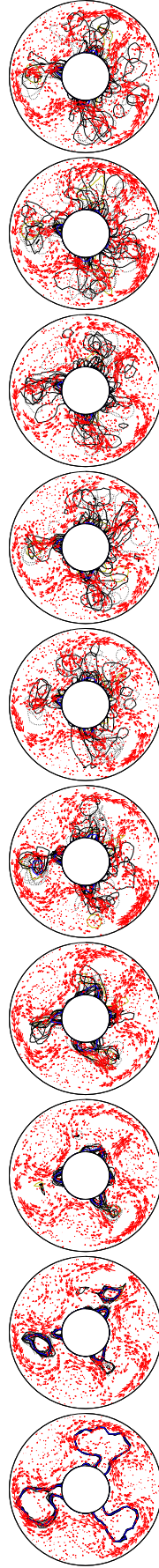
(k) Forecast F1 (3SV, $\Omega = 2.8 \text{ rad s}^{-1}$). Otherwise the same as Fig. S9k.



(l) Forecast F2. Otherwise the same as Fig. S9k.



(m) Forecast G1 (3SV, $\Omega = 3.0 \text{ rad s}^{-1}$). Otherwise the same as Fig. S9g.



(n) Forecast G2. Otherwise the same as Fig. S9m.

Figure S9: Spaghetti plots for forecasts F and G (3SV).

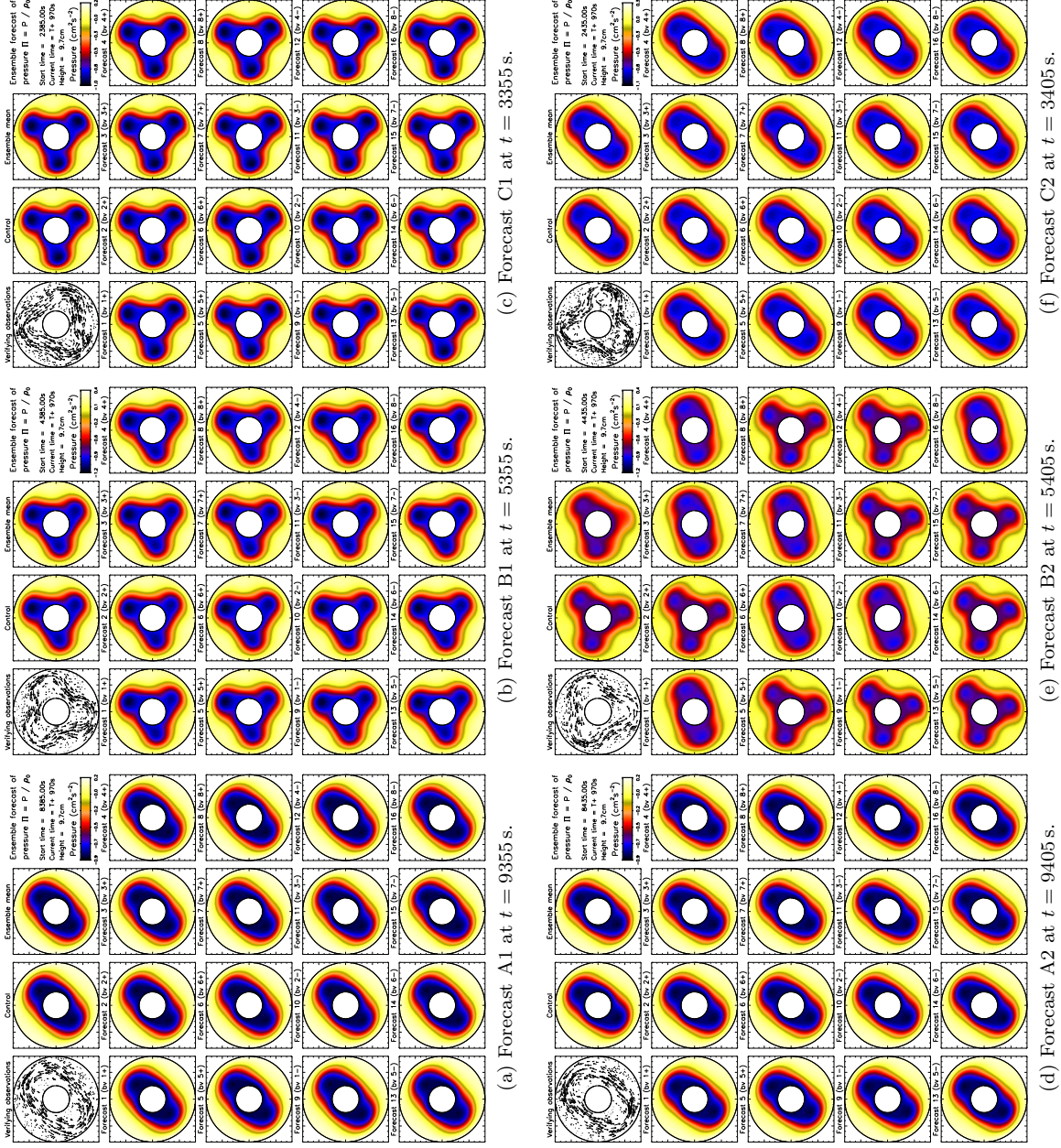


Figure S10: Ensemble forecasts for regular forecasts A, B, and C at $t_2 + 970$ s. Each frame shows the pressure field over a horizontal slice at $z = 9.7$ cm for the control forecast, ensemble mean, eight positive perturbed forecasts, and eight negative perturbed forecasts. For comparison, the observed velocity field is shown in the top left.

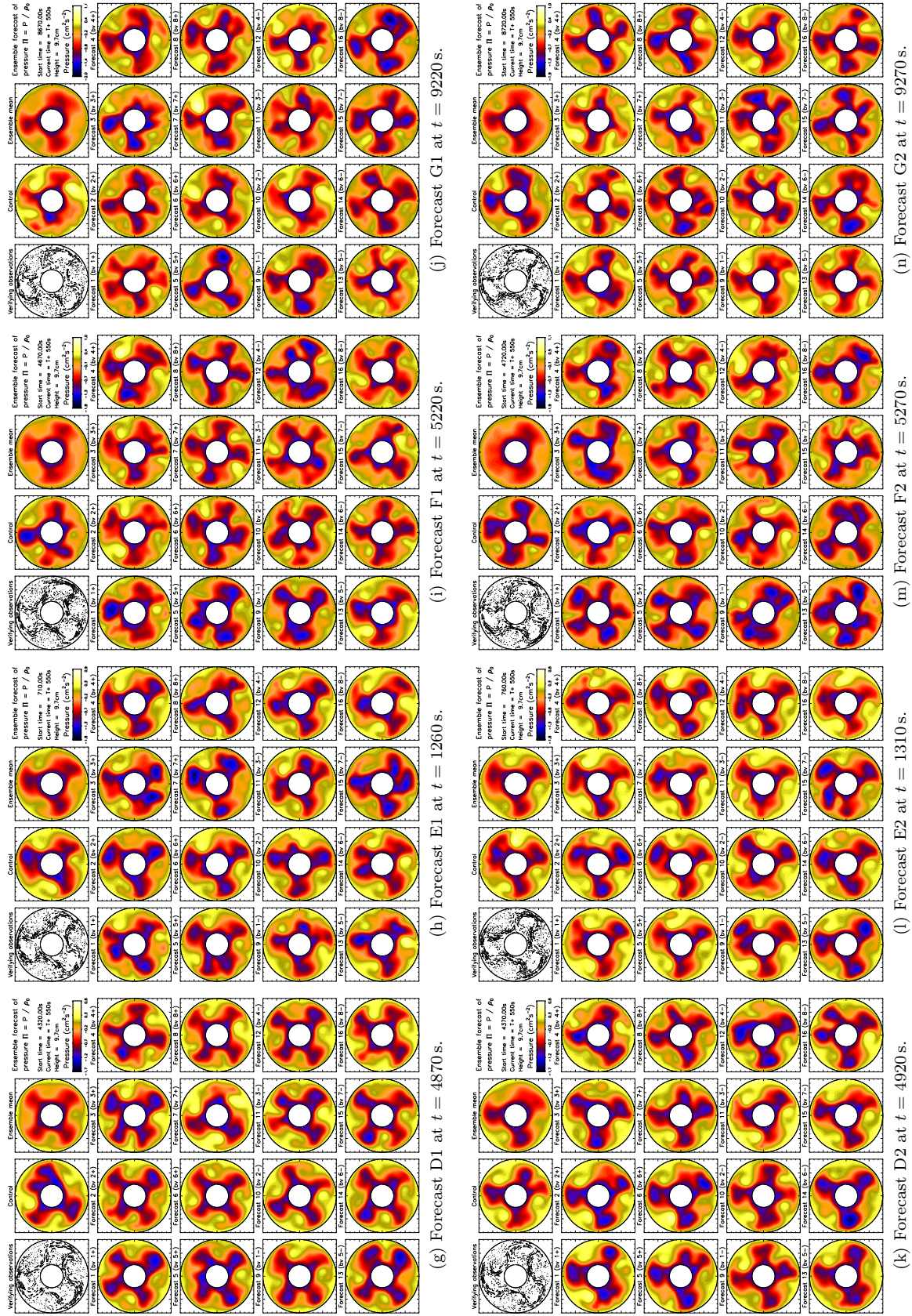


Figure S10: Ensemble forecasts for chaotic forecasts D, E, F, and G at $t_2 + 550$ s. Otherwise the same as Fig. S10.

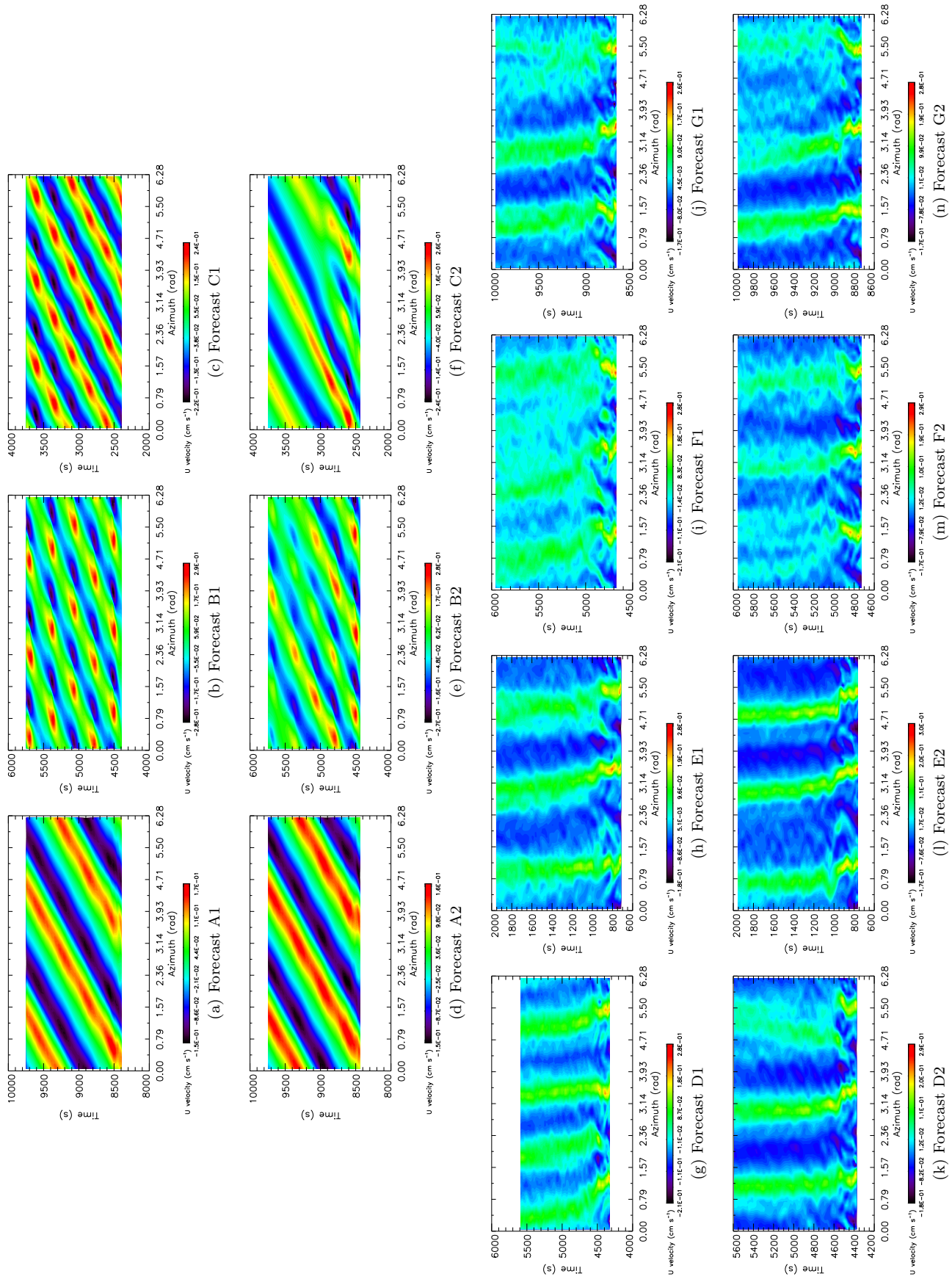


Figure S11: Hovmöller plots of the ensemble mean radial velocity for each forecast. The plots show an azimuthal circle at $R = 5.25$ cm (mid-radius) and $z = 9.7$ cm as a function of time.

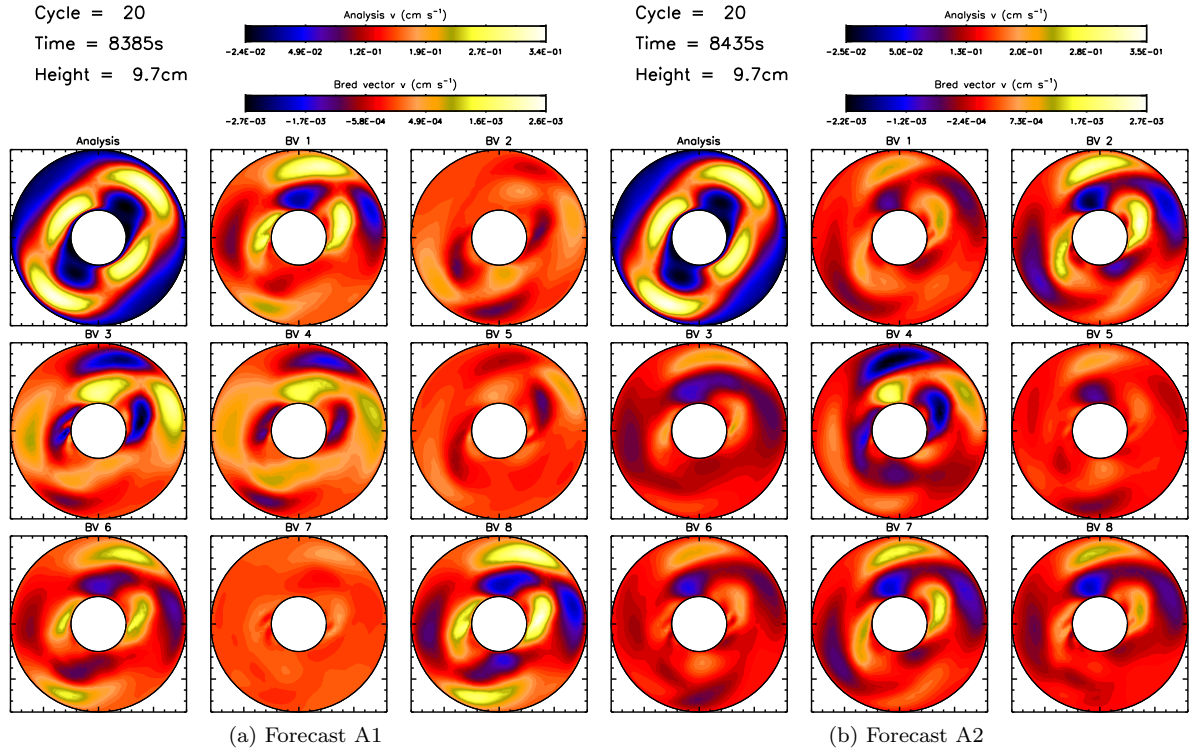


Figure S12: Azimuthal velocity breeding vectors for forecast A (2S), at the start of the forecasts ($t = t_2$). The analysis at $z = 9.7$ cm is shown in the top left, followed by the eight BVs generated by rescaling the difference between positive and negative forecasts.

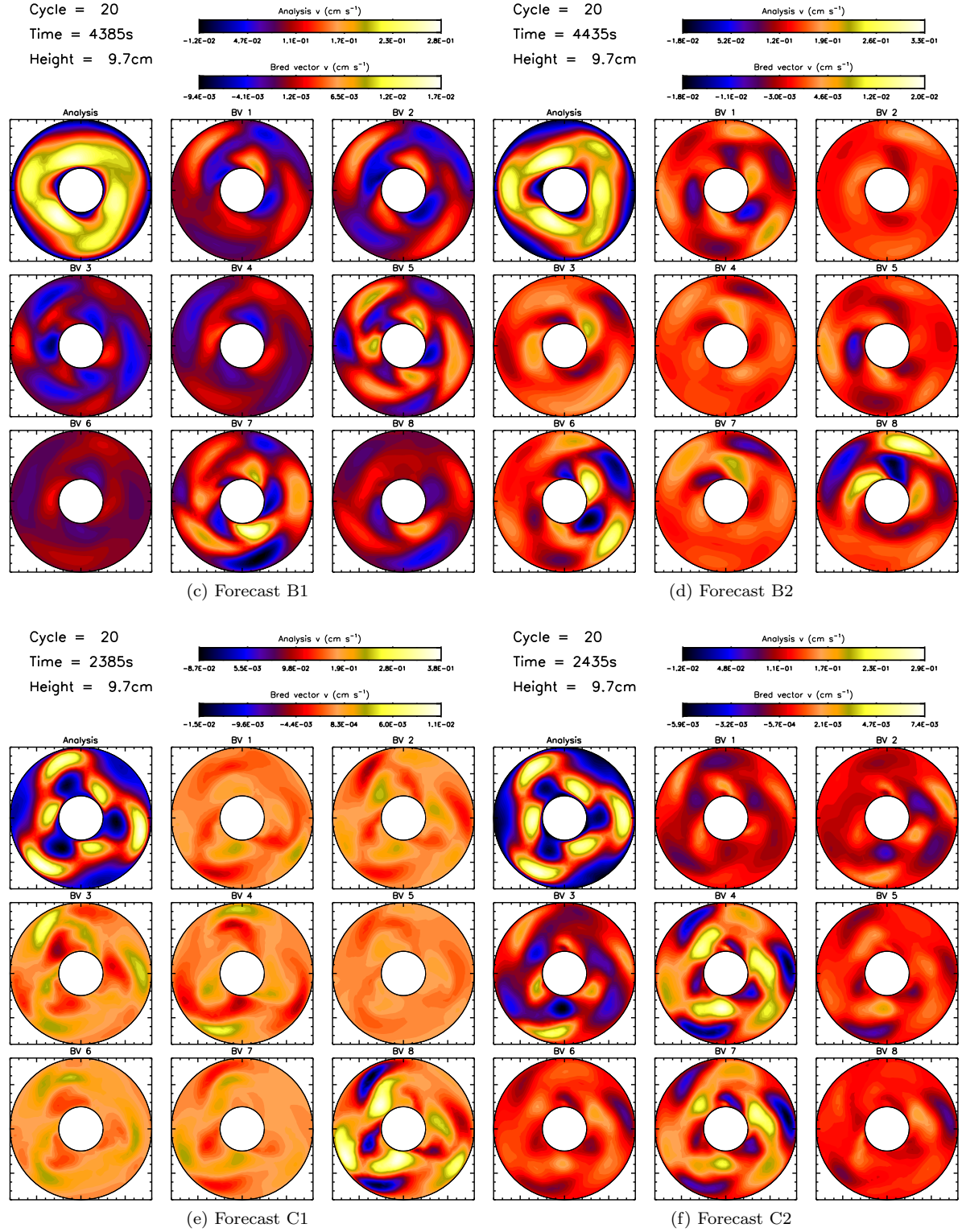


Figure S12: Continuation of previous figure — forecasts B and C (3AV).

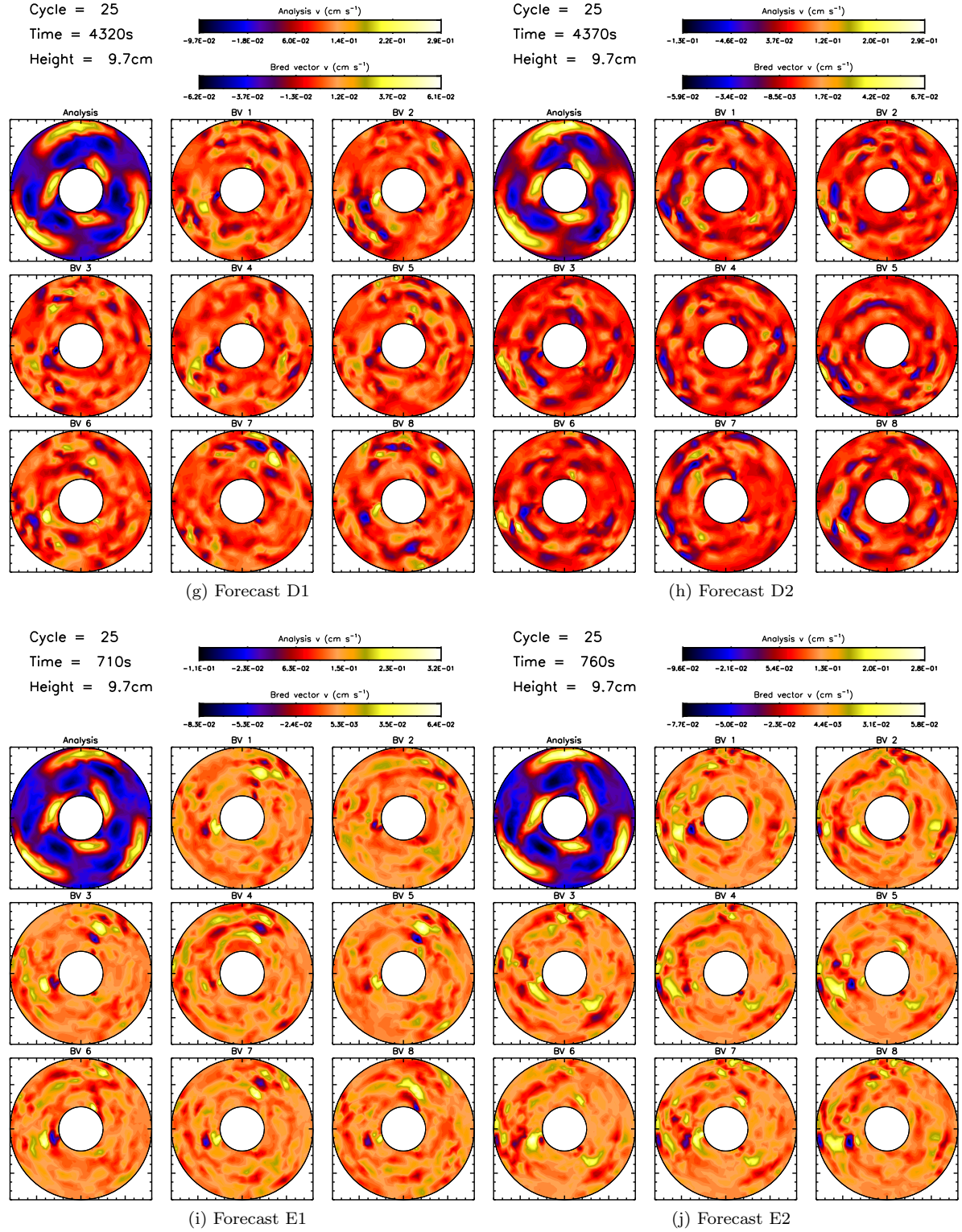


Figure S12: Continuation of previous figure — forecasts D and E (3SV).

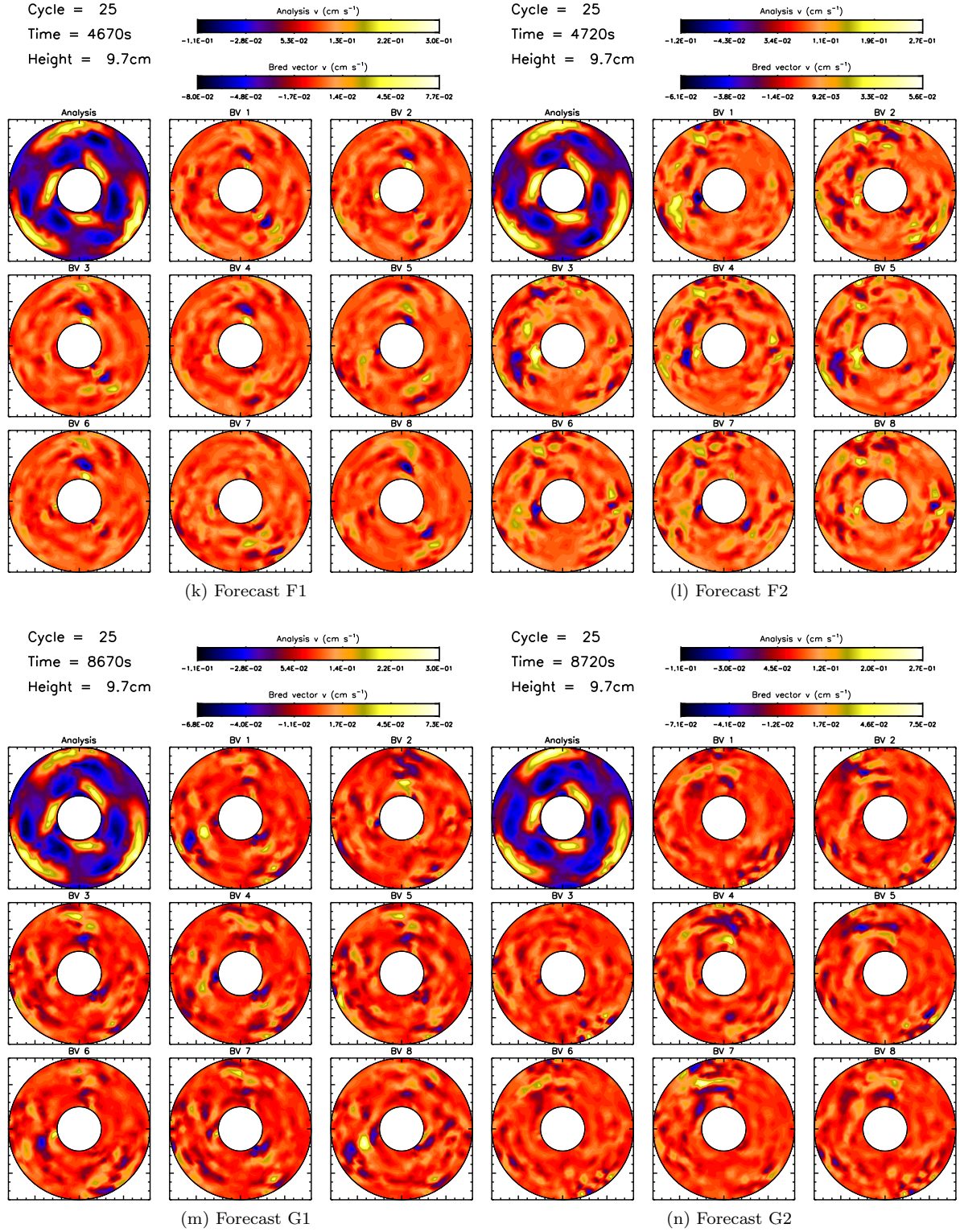


Figure S12: Continuation of previous figure — forecasts F and G (3SV).